Urban deformation monitoring using Sentinel-1 SAR data: a case study

Michele Crosetto[1], Oriol Monserrat[1], María Cuevas-González[1], Anna Barra[1],
Vrinda Krishnakumar[1], Bruno Crippa[2]

[1] Centre Tecnològic de Telecomunicacions de Catalunya (CTTC), Division of Geomatics, Av. Gauss 7, E-08860 Castelldefels (Barcelona), Spain, (mcrosetto@cttc.cat, omonserrat@cttc.cat, mcuevas@cttc.cat, abarra@cttc.cat, vkrishnakumar@cttc.cat)

[2] Dept. of Earth Sciences, University of Milan, Via Cicognara 7, I-20129 Milan, Italy, (bruno.crippa@unimi.it)

ABSTRACT

This paper describes the monitoring of the deformation associated to the construction works of a tunnel. The deformation is monitored using a Persistent Scatterer Interferometry technique and Sentinel-1 SAR data. A particular implementation of a PSI technique is described, which makes use of stable areas in the vicinity of the study area. The monitoring results include maps of accumulated deformation, to spatially describe the deformation, and deformation time series to describe the temporal evolution of deformation over the measured points.

I. INTRODUCTION

This paper concerns a case study of urban deformation monitoring based on a Persistent Scatterer Interferometry (PSI) technique, see a review in Crosetto *et al.* (2016). The case study was based on Sentinel-1 SAR data. Sentinel-1 is a constellation of two identical satellites, Sentinel-1A and Sentinel-1B, of the Copernicus Programme of the European Union. These satellites carry out C-band Synthetic Aperture Radar (SAR) data. With respect to previous European Space Agency missions (ERS-1/2 and Envisat), Sentinel-1 offers significant improvements in terms of revisiting time, spatial coverage and quality of the SAR imagery.

The Sentinel-1 satellites make use of the Interferometric Wide Swath (IWS) acquisition mode, which provides a 250-km image swath. They offer a repeat cycle of 6 days, considering both 1A and 1B. The Sentinel-1 mission has been especially designed for massive wide-area monitoring. An important advantage of the Sentinel-1 mission is that the data are freely available for both scientific and commercial applications.

The first Sentinel-1 data were acquired in 2014. Since then several studies have been devoted to urban deformation monitoring. We mention in the following the most important ones. Several studies have been devoted to monitor entire metropolitan areas. Examples include the monitoring of:

1. Mexico City [Sowter *et al.*, 2016],
2. Madrid [Bakon *et al.*, 2016],
3. Shanghai [Yu *et al.*, 2017],
4. San Francisco [Shirzaei *et al.*, 2017],
5. Beijing [Du *et al.*, 2018],
6. Ravenna [Fiaschi *et al.*, 2018],
7. and Istanbul [Aslan *et al.*, 2018].

The study of a slow-moving urban landslide area is described in Béjar-Pizarro *et al.* (2017). Kim *et al.* (2016) describe the monitoring of sink-holes in urban areas. A study of a high-speed railway bridge is described in Huang et al. (2017). Finally, the monitoring of a network of roads and railways is discussed in North *et al.* (2017).

In this paper we study the deformation associated to the construction works of a (shallow) tunnel. For this study a particular implementation of a PSI technique has been implemented. Section 2 describes the used PSI procedure. Section 3 discusses the estimation of the atmospheric component of the PSI observation, which is a key issue for PSI deformation estimation. Section 4 describes the main results of the monitoring. Section 5 includes the conclusions of the work.

II. PSI APPROACH

The authors have implemented different PSI procedures to monitor deformation, e.g. see Crosetto et al. (2011) and Devanthéry et al. (2014). For this study, we have used a particular PSI implementation. This can be used when there is a deformation area of relatively small surface, which is surrounded by stable areas. The main steps of the procedure are briefly discussed below.

The procedure starts with the acquisition of a set of N interferometric Sentinel-1 SAR images that cover the area of interest. In this work, a minimum of 25 IWS images were used. This is followed by a precise co-registration of the entire burst stack that covers the area of interest. This is basically based on the information provided by the precise orbits associated with the images.

The generation of two redundant networks of interferograms is the following step. A full-resolution

(pixel footprint: 4 by 14 m) and 10 in range by 2 in azimuth (10x2) multi-look (pixel footprint: 40 by 28 m) are generated.

Not all the PSI pixels of a given area can be exploited for interferometric purposes. The suitable pixels (which are called candidate PSs – Persistent Scatterers) are selected using the Amplitude Dispersion index proposed by Ferretti *et al.* (2000; 2001). An important processing step is given by the so-called 2+1D phase unwrapping, which is run on the redundant set of 10x2 multi-look interferograms. The algorithms and details of such a procedure are described in Devanthéry *et al.* (2014).

The identification of stable areas in the surroundings of the area of interest is another important step of the procedure. In fact, the estimation of the atmospheric component of the PSI observation is based on such areas. The atmospheric phase component is firstly estimated over the stable areas. In the current implementation of the monitoring at hand, this step is

performed assuming a linear phase model. Then a prediction and removal of the estimated atmospheric component is performed on the original single-look interferograms.

Using the set of atmospheric-free single-look interferograms, the linear deformation velocity and residual topographic component are estimated using the method of the periodogram, see for details Biescas *et al.* (2007). This is followed by the removal of the residual topographic component from the atmospheric-free single-look interferograms. Another 2+1D phase unwrapping is then performed on the set of single-look interferograms (after removing the residual topographic component and the atmospheric component).

The last two main steps of the procedure involve the generation of the final results and their geocoding: the deformation velocity and the deformation time series. These are the main products of the PSI procedure.
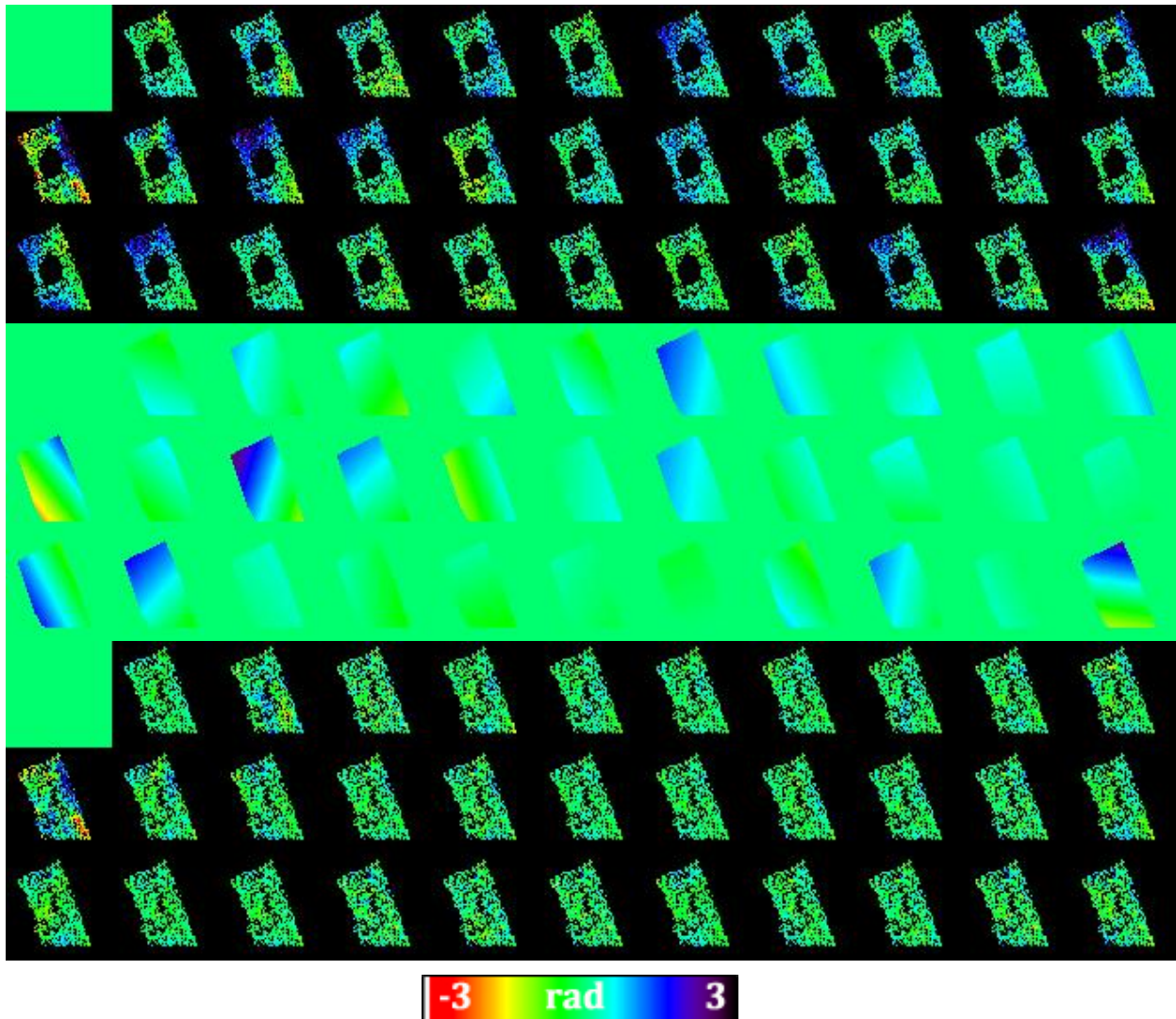

Figure 1. Atmospheric component estimation. 33 original phases that cover an area of approximately 16 km² (top). The black circles show the study area (1 km radius, approximately). Linear atmospheric components (middle). Residual phase after removing the linear atmospheric component (bottom).

Table 1. Dates of the 78 descending IWS SAR images used in this work.

#	Date	#	Date	#	Date	#	Date
1	20150306	21	20151219	41	20160827	61	20170424
2	20150318	22	20151231	42	20160908	62	20170506
3	20150330	23	20160112	43	20160920	63	20170518
4	20150411	24	20160124	44	20161002	64	20170530
5	20150505	25	20160205	45	20161014	65	20170611
6	20150517	26	20160217	46	20161026	66	20170623
7	20150529	27	20160229	47	20161107	67	20170705
8	20150610	28	20160312	48	20161119	68	20170717
9	20150704	29	20160324	49	20161201	69	20170729
10	20150716	30	20160405	50	20161213	70	20170810
11	20150728	31	20160417	51	20161225	71	20170822
12	20150809	32	20160429	52	20170106	72	20170903
13	20150821	33	20160511	53	20170118	73	20170915
14	20150914	34	20160523	54	20170130	74	20170927
15	20150926	35	20160604	55	20170211	75	20171009
16	20151008	36	20160628	56	20170223	76	20171021
17	20151101	37	20160710	57	20170307	77	20171102
18	20151113	38	20160722	58	20170319	78	20171114
19	20151125	39	20160803	59	20170331		
20	20151207	40	20160815	60	20170412		

III. Study area

The study area concerns the surroundings of a square. In this square there are important construction works, which involve the construction of a tunnel to bypass the same square. The area around this square is potentially affected by deformation due to the water pumping associated with the above construction works.

The first step of the analysis was the identification of the stable areas surrounding the area of interest. In order to define these areas, based on aquifer hydraulic properties and piezometers located in the area of interest, it was assumed that the water pumping can have a maximum influence area (i.e. the area where changes in the water table can have effect on the surface) with a radius of 1 km, centred in the middle of the square. The remaining areas, i.e. outside the influence area, were considered stable.

The analysed dataset includes 78 descending IWS SLC Sentinel-1A images, which cover the period from March 2015 to November 2017, see Table 1. Starting from these images, a set of 1813 interferograms was generated. The interferograms were generated using all possible image combinations, with a limit of 1 year for the temporal baselines.

Figure 1 illustrates the estimation and removal of the atmospheric phase component, based on stable areas. The first raw shows the original interferometric phases, which include the atmospheric component. The black circles show the study area. The second raw shows the estimated linear atmospheric components. Finally, the third row shows the residual phase after removing the linear atmospheric component.

IV. Monitoring results

In the following, we briefly discuss some monitoring results. Figure 2 shows the LOS accumulated deformation maps corresponding to the maximum of the displacement induced by water pumping (6 May 2017) and to the recovery of the displacements after stopping the water pumping (14 November 2017). From the first map it is possible to assess the actual dimension of the deformation. This information complements the in-situ measurements.

Figure 3 shows a time series that corresponds to the maximum deformation area close to the square. During the period from March to June 2017, there is a terrain subsidence (up to about -10 mm), followed by an uplift to recover to the original height. There is a good agreement between the measured time series and the piezometric data of the same area and period. This represents an example of validation of the PSI results.

Figure 4 shows another example of deformation time series. In this figure, the temperatures of the scenes are plotted in correspondence to the days of acquisition of the SAR images. There is a strong correlation between deformation and temperature. This is clearly a displacement behaviour induced by thermal expansion (Monserrat *et al.*, 2011). This type of result can be achieved only if an appropriate estimation of the atmospheric contribution is carried out: this confirms the goodness of the procedure proposed in this work.
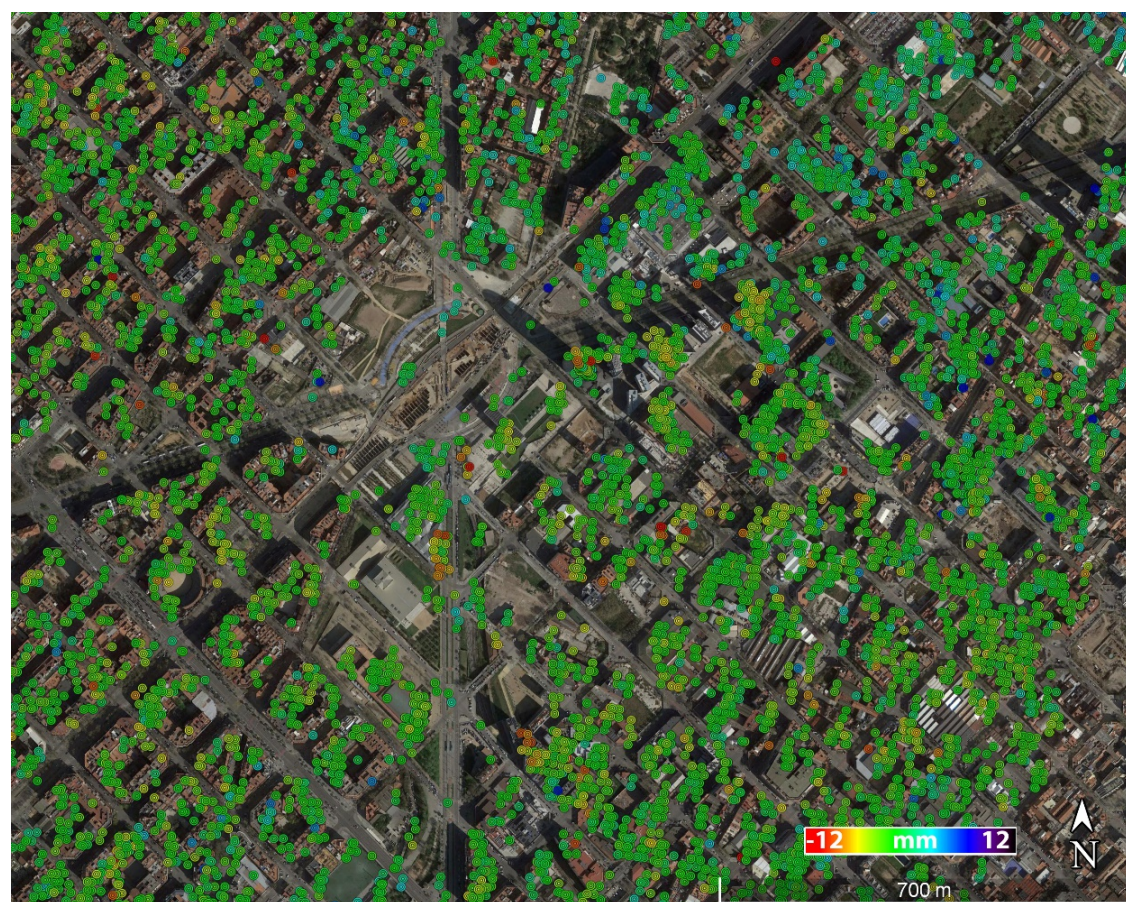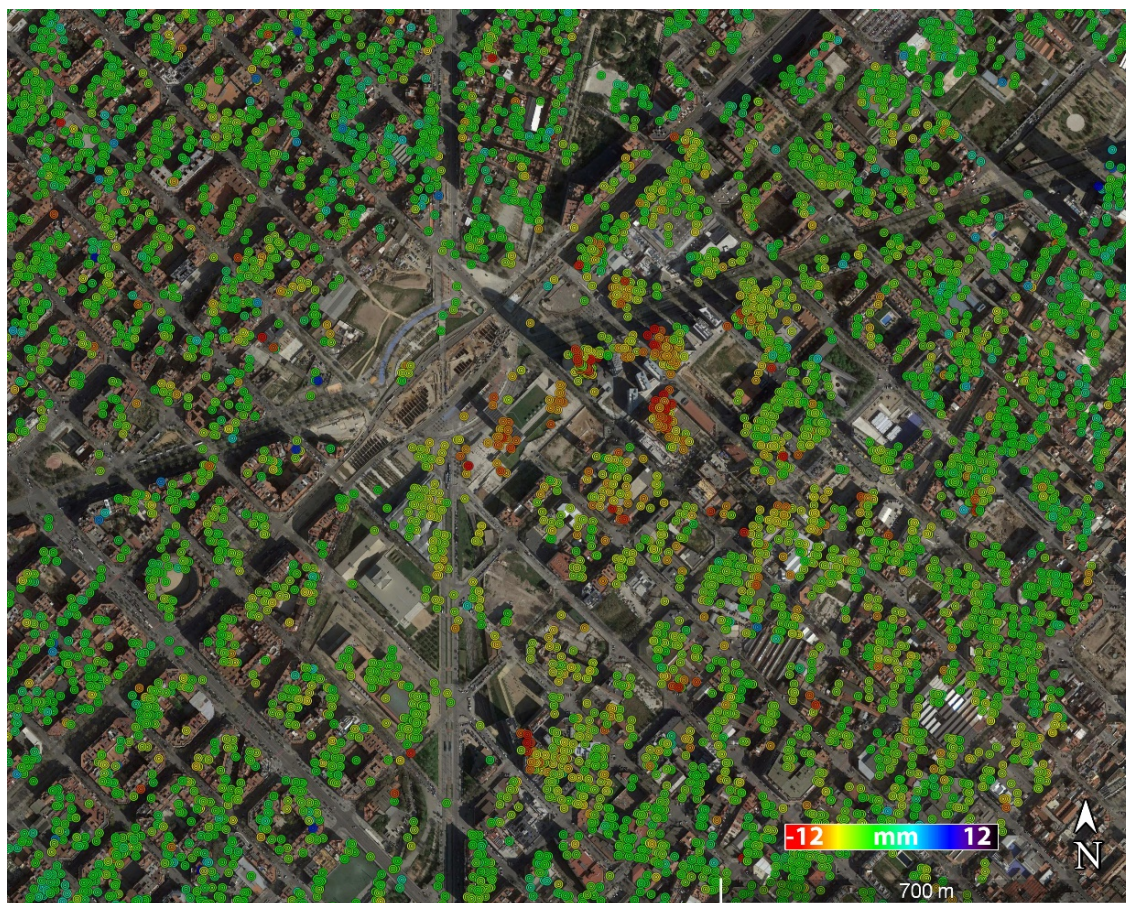
Figure 2. Cumulated deformation maps of the analysed square in correspondence to two dates: 6 May 2017 (during dewatering) and 14 November 2017, after the stopping of the water pumping.

Figure 3. Example of time series that correspond to the maximum deformation area close to the square, shown in Figure 2 (above). From March to June 2017 a terrain subsidence occurs, followed by an uplift to recover to the original height. The pattern of the deformation corresponds well to the pattern of the piezometer level of the same area, shown in red.
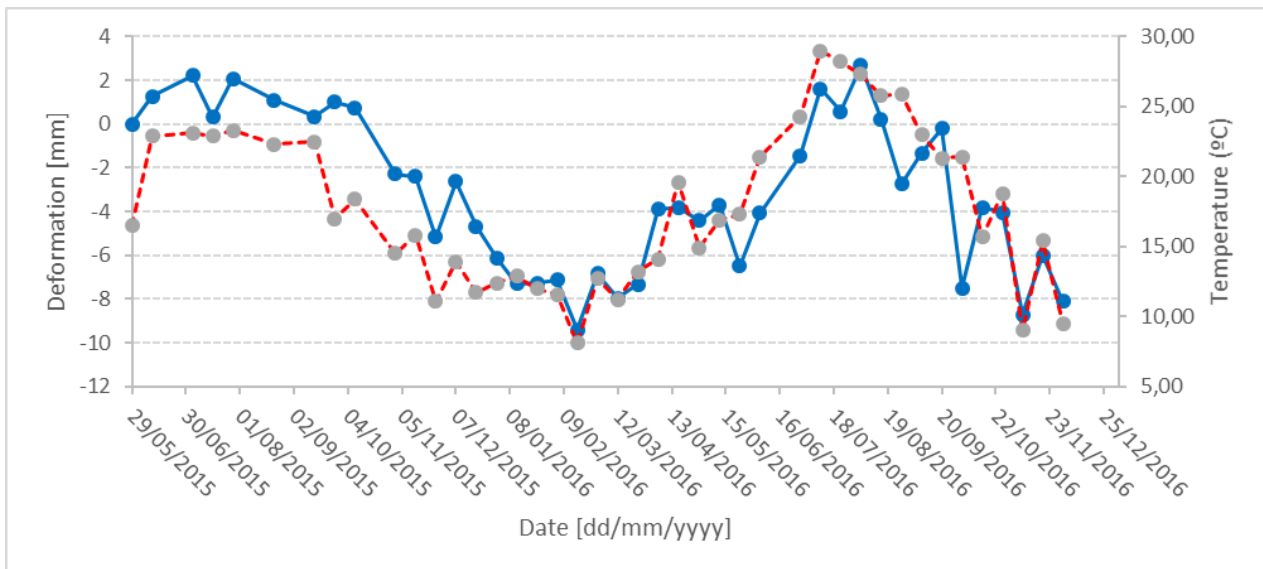

Figure 4. Example of thermal expansion displacement. The displacement time series (blue line) has a similar pattern of the temperatures at the time of acquisition of the SAR images (red line).

V. CONCLUSIONS

In this paper a monitoring case study has been described, which concerns the deformation associated to the construction works of a tunnel. The deformation monitoring has been based on a PSI technique and Sentinel-1 SAR data. In the paper, a particular implementation of a PSI technique has been described, which makes use of stable areas in the vicinity of the study area at hand. The stable areas are used to estimate the atmospheric phase component, which is then removed from the original PSI observations.

Interesting monitoring results have been obtained. The maps of accumulated deformation allow us to achieve a spatial description of the deformation, which complements the information provided by the in-situ measurements that are more concentrated in the construction work area (basically including the square and its close vicinity).

Two examples of deformation time series have been discussed. In the first one a good agreement between the deformation time series and a piezometric level has been shown. This represents a validation of the PSI results.

In addition, an example of thermal expansion has been described. This illustrates the high sensitivity of the technique to small displacements and confirms the goodness of the strategy proposed in this work to remove the atmospheric component.

The proposed PSI procedure has been tested for a specific application, i.e. the monitoring of urban land deformation caused by water extraction. However, the procedure can work with any type of deformation phenomena, provided that its spatial extension is sufficiently small. In fact, the proposed procedure works only over relatively small areas, where the atmospheric component, estimated over the stable

areas, can be interpolated in the area of interest. The larger is the area of interest, the bigger will be the error in the estimation of the atmospheric component over this area.

VI. ACKNOWLEDGEMENTS

References

Aslan, G.; Cakır, Z.; Ergintav, S.; Lasserre, C.; Renard, F. Analysis of Secular Ground Motions in Istanbul from a Long-Term InSAR Time-Series (1992–2017). *Remote Sens*, 2018, 10(3), 408.

Bakon, M.; Marchamalo, M.; Qin, Y.; García-Sánchez, A.J.; Alvarez, S.; Perissin, D.; Papco, J.; Martínez, R. Madrid as Seen from Sentinel-1: Preliminary Results. *Procedia Comput Sci*, 2016, 100, 1155-1162.

Biescas E.; Crosetto M.; Agudo M.; Monserrat O.; Crippa B. Two radar interferometric approaches to monitor slow and fast land deformations. *Journal of Surveying Engineering*, 2007, 133 (2), 66-71.

Béjar-Pizarro, M.; Notti, D.; Mateos, R.M.; Ezquerro, P.; Centolanza, G.; Herrera, G.; Bru, G.; Sanabria, M.; Solari, L.; Duro, J.; Fernández, J. Mapping Vulnerable Urban Areas Affected by Slow-Moving Landslides Using Sentinel-1 InSAR Data. *Remote Sens*, 2017, 9(9), 876.

Crosetto, M., Monserrat, O., Cuevas, M. and Crippa, B. "Spaceborne Differential SAR Interferometry: Data Analysis Tools for Deformation Measurement". *Remote Sens* 2011, 3, 305-318;

Crosetto, M.; Monserrat, O.; Cuevas-González, M.; Devanthéry, N.; Crippa, B. Persistent Scatterer Interferometry: a review. *ISPRS J Photogramm Remote Sens*, 2016, 115, 78-89.

Devanthéry, N.; Crosetto, M.; Monserrat, O.; Cuevas-González, M.; Crippa, B. An approach to Persistent Scatterer Interferometry. *Remote Sens*, 2014, 6, 6662-6679.

Du, Z.; Ge, L.; Ng, A.H.M.; Xiaojing, L.; Li, L. Mapping land subsidence over the eastern Beijing city using satellite radar interferometry. *Int J Digital Earth*, 2018, 11(5), 504-519.

Ferretti, A.; Prati, C.; Rocca, F. Nonlinear subsidence rate estimation using permanent scatterers in differential SAR interferometry. *IEEE Trans Geosci Remote Sens*, 2000, 38, 2202–2212.

Ferretti, A.; Prati, C.; Rocca, F. Permanent scatterers in SAR interferometry. *IEEE Trans Geosci Remote Sens*, 2001, 39, 8–20.

Fiaschi, S.; Tessitore, S.; Bonì, R.; Di Martire, --D.; Achilli, V.; Borgstrom, S.; Ibrahim, A.; Floris, M.; Meisina, C.; Ramondini, M.; Calcaterra, D. From ERS-1/2 to Sentinel-1: two decades of subsidence monitored through A-DInSAR techniques in the Ravenna area (Italy). *GIsci Remote Sens*, 2017, 54(3), 305-328.

Huang, Q.; Crosetto, M.; Monserrat, O.; Crippa, B. Displacement monitoring and modelling of a high-speed railway bridge using C-band Sentinel-1 data. *ISPRS J Photogramm Remote Sens*, 2017, 128, 204-211.

Kim, J.W.; Lu, Z.; Degrandpre, K. Ongoing deformation of sinkholes in Wink, Texas, observed by time-series Sentinel-1a SAR interferometry (preliminary results). *Remote Sens*, 2016, 8(4), 313.

Monserrat, O.; Crosetto, M.; Cuevas, M.; Crippa, B. The Thermal Expansion Component of Persistent Scatterer Interferometry Observations. *IEEE Geosci Remote S*, 2011, 8 (5), 864-868.

North, M.; Farewell, T.; Hallett, S.; Bertelle, A. Monitoring the Response of Roads and Railways to Seasonal Soil Movement with Persistent Scatterers Interferometry over Six UK Sites. *Remote Sens*, 2017, 9(9), 922.

Shirzaei, M.; Bürgmann, R.; Fielding, E.J. Applicability of Sentinel-1 Terrain Observation by Progressive Scans multitemporal interferometry for monitoring slow ground motions in the San Francisco Bay Area. *Geophys Res Lett*, 2017, 44(6), 2733-2742.

Sowter, A.; Amat, M.B.C.; Cigna, F.; Marsh, S.; Athab, A.; Alshammari, L. Mexico City land subsidence in 2014–2015 with Sentinel-1 IW TOPS: Results using the Intermittent SBAS (ISBAS) technique. *Int J Appl Earth Obs Geoinf*, 2016, 52, 230-242.

Yu, L.; Yang, T.; Zhao, Q.; Liu, M.; Pepe, A. The 2015–2016 Ground Displacements of the Shanghai coastal area Inferred from a combined COSMO-SkyMed/Sentinel-1 DInSAR Analysis. *Remote Sens*, 2017, 9(11), 1194.